Split-Lohmann Multifocal Displays (Supplemental Material)

YINGSI QIN, WEI-YU CHEN, MATTHEW O'TOOLE, and ASWIN C. SANKARANARAYANAN, Carnegie Mellon University, USA

ACM Reference Format:
Yingsi Qin, Wei-Yu Chen, Matthew O'Toole, and Aswin C. Sankaranarayanan. 2023. Split-Lohmann Multifocal Displays (Supplemental Material). *ACM Trans. Graph.* 42, 4 (August 2023), 6 pages. https://doi.org/10.1145/3592110

S1 DETAILED DERIVATION OF IMAGE FORMATION MODEL

S1.1 Preliminaries

Much of our system design relies on basic properties of 4f systems, which we state here for completeness. The interested reader is referred to Goodman's book for additional details.

A 4f relay refers to the arrangement shown in Figure S1; here, a wavefront described in terms of a phasor field $u_1(x_1, y_1)$ is incident on the plane marked as P_1; two lenses, which we assume have the same focal length of f_0 m, are placed at a distance of f_0 and $3f_0$ from the plane P_1. We identify the planes P_2 and P_3 as those at a distance $2f_0$ and $4f_0$ respectively from P_1. When the two lenses that comprise the relay are ideal thin lenses, and there is no optical element at P_2, then the phase field at P_3, denoted as $u_3(x_3, y_3)$, is given as,

$$u_3(x_3, y_3) = u_1(-x_3, -y_3). \tag{1}$$

Specifically, except for the reversal along the x and y axes, the 4f system acts as an *ideal wavefront relay*—a feature that makes it invaluable in imaging systems to propagate wavefronts without any aberrations.

Now suppose we introduce a thin modulation element at P_2, which multiplies the field element-wise at P_2 by a term $p(x_2, y_2)$; in this configuration, the output field at P_3 is given as

$$u_3(x_3, y_3) = u_1(-x_3, -y_3) * P\left(\frac{x_3}{\lambda f_0}, \frac{y_3}{\lambda f_0}\right), \tag{2}$$

where $P(u, v)$ is the two-dimensional Fourier transform of $p(x, y)$, and $*$ denotes the convolution operator.

There are two instances of aperture functions $p(\cdot, \cdot)$ that we use in this work. We briefly discuss them next.

Authors' address: Yingsi Qin, yingsiq@andrew.cmu.edu; Wei-Yu Chen, weiyuc@andrew.cmu.edu; Matthew O'Toole, mpotoole@cmu.edu; Aswin C. Sankaranarayanan, saswin@andrew.cmu.edu, Carnegie Mellon University, 5000 Forbes Ave, Pittsburgh, PA, 15213, USA.

0730-0301/2023/8-ART
https://doi.org/10.1145/3592110

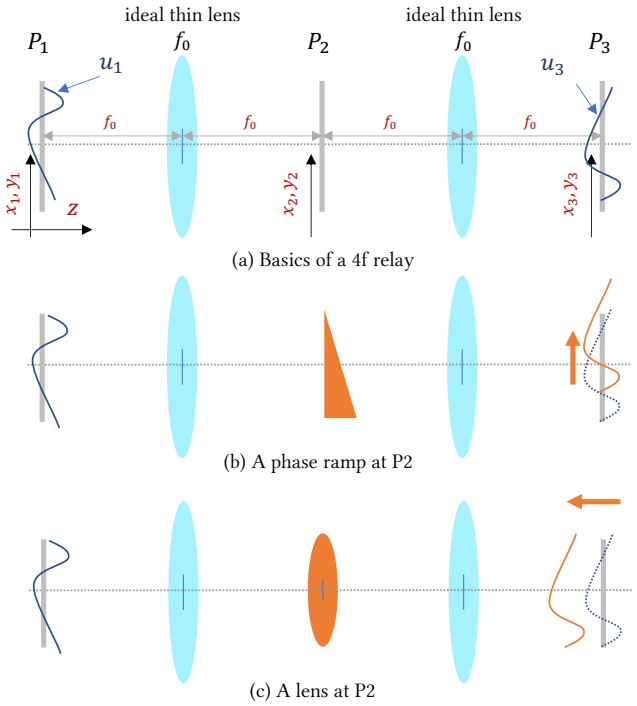

Fig. S1. Basics of a 4f system. (a) A 4f system consists of two lens, here with the same focal length f_0, placed $2f_0$ from each other; identifying the planes P_1, P_2, and P_3 as shown in the figure, the 4f system behaves as a wave relay, allowing for an incident field at P_1 to be reproduced at P_3, except for a flip along the x and y axes. (b) A phase ramp—or a linear phase shift—introduced at P_2 results in a *lateral* shift of the field at P_3. (c) A lens—or a quadratic phase shift—introduced at P_2 results in a *axial* shift of the field at P_3.

Linear phase modulation in P_2. Suppose that $p(x_2, y_2)$ is a linear phase function of the form

$$p_{\text{lin}}(x_2, y_2) = e^{-j\frac{2\pi}{\lambda}(x_2 u_0 + y_2 v_0)}.$$

From basic Fourier properties, we get

$$P_{\text{lin}}(u, v) = \delta\left(u + \frac{u_0}{\lambda}, v + \frac{v_0}{\lambda}\right).$$

In this scenario, Eq. (2) becomes

$$u_3(x_3, y_3) = u_1(-x_3, -y_3) * \delta\left(x_3 + u_0 f_0, y_3 + v_0 f_0\right) \tag{3}$$

$$= u_1(-x_3 + u_0 f_0, -y_3 + v_0 f_0). \tag{4}$$

Hence, a linear phase ramp in the P_2 leads to a shift of the wavefront in P_3. For analytical tractability, we ignore the effects of any limiting apertures here and in rest of the analysis.

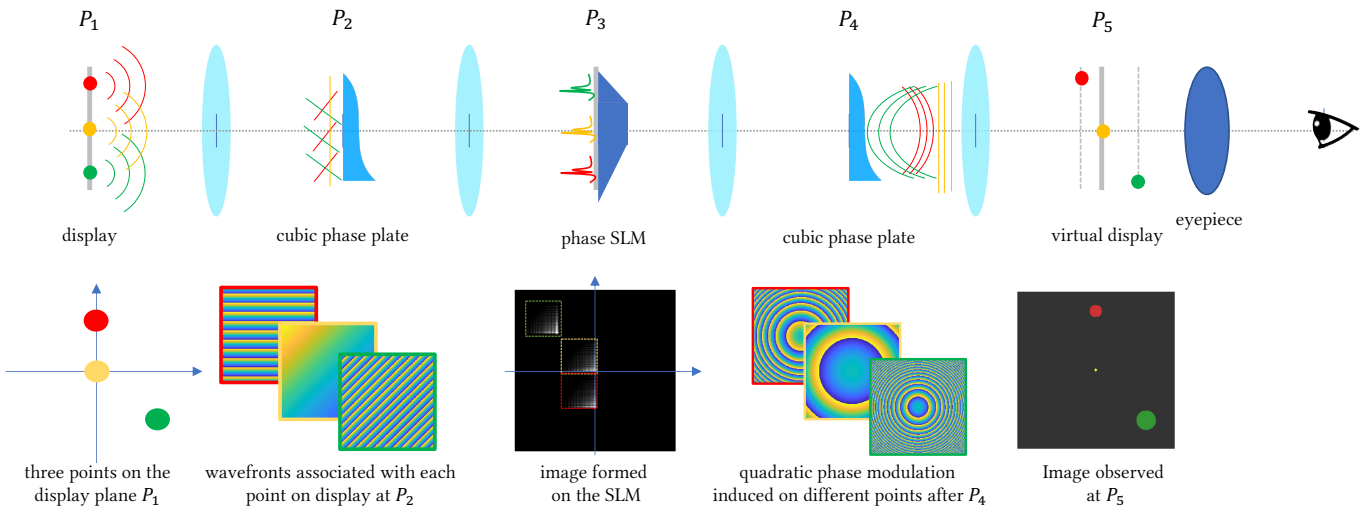

Fig. S2. **Analysis of Split-Lohmann multifocal displays.** The figure illustrates the propagation of waves from three distinct points, color-coded for visualization. All points start at the display as ideal point light sources, incoherent with each others, and are collimated with plane waves when they are incident on the first cubic phase plate at P_3. At the SLM placed at P_3, the phase gradient observed by each is different, i.e., the choice of v_0 in Eq. (11) is different: zero for the yellow point, a small positive value for the red, and a larger negative value for the green point. This results in different amounts of shifts between the interfering cubic wavefronts at P_4; the resulting waves after the second cubic plate is planar, converging quadratic and diverging quadratic for yellow, red, and green points, respectively. As a consequence, each point undergoes a different amount of axial shift at the P_5, where the translating virtual display is formed.

Quadratic phase modulation in P_2. Suppose that we place a lens in P_2, i.e., $p(x_2, y_2)$ takes the form

$$p_{\text{quad}}(x_2, y_2) = e^{-j\frac{2\pi}{\lambda}\frac{x_2^2+y_2^2}{2f_t}},$$

where f_t is the focal length of the lens. Again, from basic Fourier properties, we get

$$P_{\text{quad}}(u, v) = \frac{\lambda f_t}{-j} e^{j\pi(u^2+v^2)(\lambda f_t)},$$

and Eq. (2) becomes

$$u_3(x_3, y_3) \propto u_1(-x_3, -y_3) * e^{j\frac{2\pi}{\lambda}\frac{f_t}{2f_0^2}(x_3^2+y_3^2)}. \tag{5}$$

Comparing this to wave propagation under Fresnel approximation, we can interpret the $u(x_3, y_3)$ to be the wave $u_1(-x_3, -y_3)$ propagated by a distance $\delta_z = f_0^2/f_t$. Specifically, if we did not have a lens in P_2, or set $f_t = \infty$, then we would observe the field $u_1(-x_3, -y_3)$ at P_3; adding a lens with focal length f_t translates the field *axially* by a distance δ_z towards the second lens. Or as stated in the main paper, the field $u_1(-x_3, -y_3)$, instead of appearing at $z = 4f_0$, now appears at

$$z = 4f_0 + \delta_z = 4f_0 - f_0^2/f_t. \tag{6}$$

S1.2 Image Formation in Split-Lohmann Displays

We now provide a detailed breakdown of wavefront propagation and image formation in Split-Lohmann displays. This analysis will also touch upon the different sources of non-idealities in the design and provide a mechanism to reason about their effects. Specifically, we derive wavefronts formed at different locations in the system—labeled as the planes $P_1, \ldots, P_5$—as light propagates from the display and to the eye; each plane is $2f_0$ from its preceding one. A visual overview of this analysis in provided in the Figure S2.

P_1: Display. We assume a display with spatially incoherent pixels, but temporally coherent at a wavelength λ. *Spatial incoherence allows us to analyze the pixels in isolation, since their wavefronts do not interfere.* In terms of implementation, an OLED display provides us with a good approximation to this model.

Consider a point at a location (x_0, y_0) on the display, and track its wavefront through the system. Mathematically, we will model it with a delta function as follows:

$$u_1(x_1, y_1) = \delta(x_1 - x_0, y_1 - y_0) \tag{7}$$

To help visualize the wavefronts, a few such points are highlighted with different colors in Figure S2.

P_2: The first cubic phase plate. The first lens collimates the light from a point on P_1, and so *we expect to see a plane wave at P_2*. Since we are tracking the wavefront associated with a point source at (x_0, y_0), the wavefront at P_2, prior to the cubic phase plate is given as

$$u_{2,-}(x_2, y_2) = \frac{1}{\lambda f_0} e^{-j\frac{2\pi}{\lambda}\frac{x_2 x_0 + y_2 y_0}{f_0}} \tag{8}$$

The cubic phase plate changes this wavefront to

$$u_{2,+}(x_2, y_2) = u_{2,-}(x_2, y_2) e^{-j\frac{2\pi}{\lambda}\frac{x_2^3+y_2^3}{c_0}} \tag{9}$$

Here, c_0 is a parameter that determines the curvature of the phase plate; we will discuss constraints on it value in the next section.

P_3: Phase SLM. The wavefront at P_3 is estimated by noting that P_3 is 4f away from P_1, with a bicubic phase function at its pupil/Fourier plane at P_2. If we denote $h(\cdot,\cdot)$ as the Fourier transform of the cubic phase plate, then the wavefront prior to the SLM placed at P_3 is given as

$$u_{3,-}(x_3, y_3) = h(x_3 + x_0, y_3 + y_0). \tag{10}$$

That is, we observe a copy of $h(x, y)$ at the location $(-x_0, -y_0)$. This wavefront is phase modulated by the SLM.

As motivated earlier, the phase modulation at the SLM is piecewise linear. However, the spatial extent of $h(\cdot,\cdot)$ complicates any subsequent analysis, since it is entirely likely that the wavefront, or the region where most of its energy is concentrated, is potentially spreads across two or more linear pieces. To retain tractability in our analysis, we assume that is not the case and that the wavefront u_{3-} encounters only a single phase ramp in the region where its energy is concentrated; as noted earlier, this corresponds to a region with length and width of approximately 100 µm in our setup. We will discuss aberrations introduced when this assumption is violated shortly.

Under this assumption, the wavefront after the SLM becomes

$$u_{3,+}(x_3, y_3) = u_{3,-}(x_3, y_3) e^{-j\frac{2\pi}{\lambda}(x_3+y_3)v_0}. \tag{11}$$

Here, v_0 is the slope parameter that controls the amount of shift we induce on the wavefront at P_4. As discussed in Section 2.2, Lohmann lenses require the same amount of shift along both axes and hence, we use the same slope parameter v_0 for both x and y. The specific choice of v_0 is determined by the depth map we seek to show; we will discuss this in more detail later.

P_4: The second cubic phase plate. Under the assumptions made on the wavefront at P_3 being concentrated into a single linear piece of the SLM, the optical path from $u_{2,+}$ to $u_{4,-}$ is one of a 4f system with a linear phase ramp in its Fourier plane; hence, the wavefront prior to the second cubic phase plate is a translated copy of the one at P_2. Denoting $\Delta = v_0 f_0$, from Eq. (4), we can write this as

$$u_{4,-}(x_4, y_4) = u_{2,+}(-x_4 + \Delta, -y_4 + \Delta) \tag{12}$$

$$= u_{2,-}(-x_4 + \Delta, -y_4 + \Delta) e^{-j\frac{2\pi}{\lambda}\frac{(-x_4+\Delta)^3+(-y_4+\Delta)^3}{c_0}} \tag{13}$$

Since $u_{2,-}$ corresponds to a planar wavefront, its translation only changes it by a constant/scalar. After the second cubic phase plate, the wavefront becomes

$$u_{4,+}(x_4, y_4) = u_{3,+}(x_4, y_4) e^{-j\frac{2\pi}{\lambda}\frac{x_4^3+y_4^3}{c_0}} \tag{14}$$

$$= u_{2,-}(-x_4 + \Delta, -y_4 + \Delta) \times \cdots \tag{15}$$

$$e^{-j\frac{2\pi}{\lambda}\frac{(-x_4+\Delta)^3+(-y_4+\Delta)^3}{c_0}} e^{-j\frac{2\pi}{\lambda}\frac{x_4^3+y_4^3}{c_0}} \tag{16}$$

After some simplifications, the wavefront $u_{4,+}(x_4, y_4)$ can be written as

$$\underbrace{u_{2,-}(-x_4 + \Delta, -y_4 + \Delta)}_{\text{(plane wave from display)}} \underbrace{e^{-j\frac{2\pi}{\lambda}\frac{3\Delta(x_4^2+y_4^2)}{c_0}}}_{\text{(quadratic phase term)}} \underbrace{e^{j\frac{2\pi}{\lambda}\frac{3\Delta^2(x_4+y_4)}{c_0}}}_{\text{(linear phase term)}} \tag{17}$$

In simpler words, the wavefront after the second cubic phase plate is the same as the one *before* the first cubic plate, multiplied by two phase terms: a quadratic term corresponding to a lens with focal length $f_t = c_0/(6\Delta) = c_0/(6v_0 f_0)$, and a linear term.

P_5: Virtual display plane. If we ignore the quadratic and linear phase terms in Eq. (17), then the wavefront at P_5 is the same as the one in P_1—a delta function centered at (x_0, y_0). The quadratic phase term induces an axial shift $\delta_z = -f_0^2/f_t$, as derived in Eq. (6), and so this delta function appears at a location of

$$\delta_z = -\frac{6v_0 f_0^3}{c_0}, \tag{18}$$

with respect to P_5 plane, with negative values indicating displacements away from the eyepiece. Recall, that we control v_0 via the phase patterns shown on the SLM, and so via judicious choice of this value, we can place a point at a different axial distance from the eyepiece, which in turn allows the eye to perceive it as arising from a desired depth.

The linear phase term provides a lateral shift so that the delta function appears at

$$\left(x_0 - \frac{3v_0^2 f_0^3}{c_0}, y_0 - \frac{3v_0^2 f_0^3}{c_0}\right). \tag{19}$$

This lateral shift is undesired, but is often very small due to its dependence on v_0^2; we discuss it in more detail later in this section.

S1.3 Axial Placement of the Eye

Figure S3 provides ray diagrams that describe the importance of eye placement. Our display produces correct content when the eye is placed at the focal plane of the eyepiece, i.e., at a distance from the eyepiece equal to its focal length. When the eye is displaced from the focal plane, then there is an undesirable lateral shift when the display places content at different depths. Empirically, we observe this manifest in the form of breathing artifacts where the scene seems to expand or contract when we perform a focus sweep.

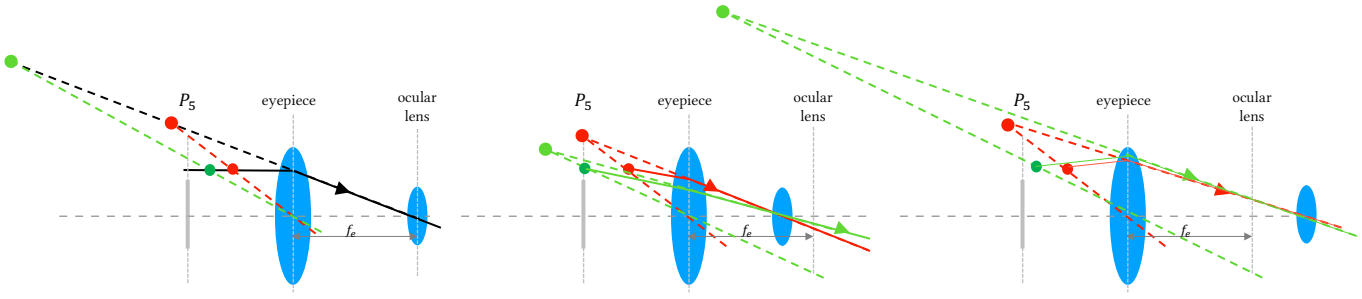

(a) Eye placed at eyepiece's focal plane (a) Eye placed closer than the focal plane (a) Eye placed beyond the focal plane

Fig. S3. **Axial placement of the eye.** Our system requires that the eye be placed at the focal plane of the eyepiece for appropriate observation of focus cues. (a) When the eye is placed at the eyepiece's focal plane, axial translation of a displayed scene content results in it being observed at different depths. Here, the green point is to be placed further away than the red one. (b, c) If the eye not placed at the focus plane, then there is a lateral change in where the point is observed. Visually, this appears in the form of "focus breathing" artifacts, where scene points drift spatially under defocus.

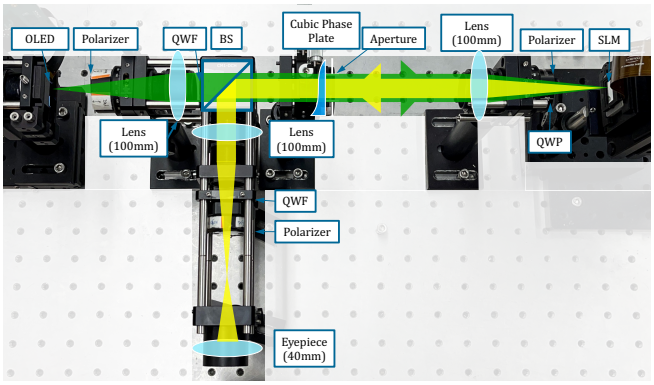

Component	Manufacturer	Part Number
OLED	SEEYA	SY103WAM01
SLM	Holoeye	GAEA-2
Cubic Phase Plate	Power Photonic	Customized
Lenses	Thorlabs	AC254-100-A
Eyepiece	Thorlabs	TRH254-040-A
Aperture	Thorlabs	SM1D12C
Beam Splitter	Thorlabs	BS004
Polarizers	Thorlabs	LPVISE2X2
$\lambda/4$ Plate (QWP)	Thorlabs	AQWP10M-580
$\lambda/4$ Film (QWF)	Edmund Optics	14-723

Fig. S4. Detailed schemaic and component layout of our lab prototype.

S2 ADDITIONAL HARDWARE PROTOTYPE DETAILS

S2.1 Hardware Specifications

Here we show our complete setup and list all components we used in Figure S4. In comparison with Figure 9, we add several linear polarizers and quarter-wave plates/films. These components are used to remove ghosting caused by light directly reflected from the coating of the cubic phase plate.

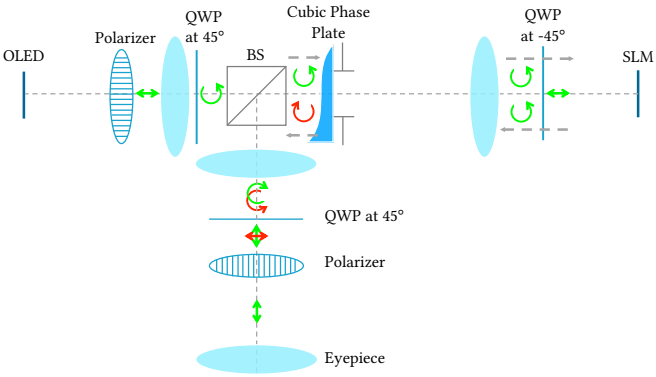

Fig. S5. Illustration of reflection removal from the cubic phase plate using the double pass technique. The pass light is labeled in green and the reflection from the cubic phase plate is labeled in red. When reflected from the cubic phase plate, the right-hand circularly polarized light gets reflected once more by the beam splitter, yielding left-hand circularly polarized light that meets the final retarder. The resulting linearly polarized at 135° is thus blocked by the final polarizer at 45°.

Ghosting removal. The key idea is to make the ghosting polarized differently with the correct light path. As explained in Figure S5, we first circularly polarized light by a polarizer and a QWP. When it hits the surface of the cubic phase plate, most of the light (green) will correctly transmit, but few lights will be reflected (red) and thus causing ghosting. By adding another QWP before the SLM, the correct light path will hit the QWP twice, and thus reverse the direction of circular polarization. In the end, the correct light path and the ghosting are both circularly polarized, but in the reversed direction. After passing through a 45-degree QWP, they are linearly polarized in an orthogonal direction and thus can be separated by another linear polarizer.

Fabrication of Cubic Phase Plate. The cubic phase plate was custom fabricated by Power Photonic using fused silica as the substrate (refractive index $n = 1.4585$) and with $c_0 = 0.0193$.

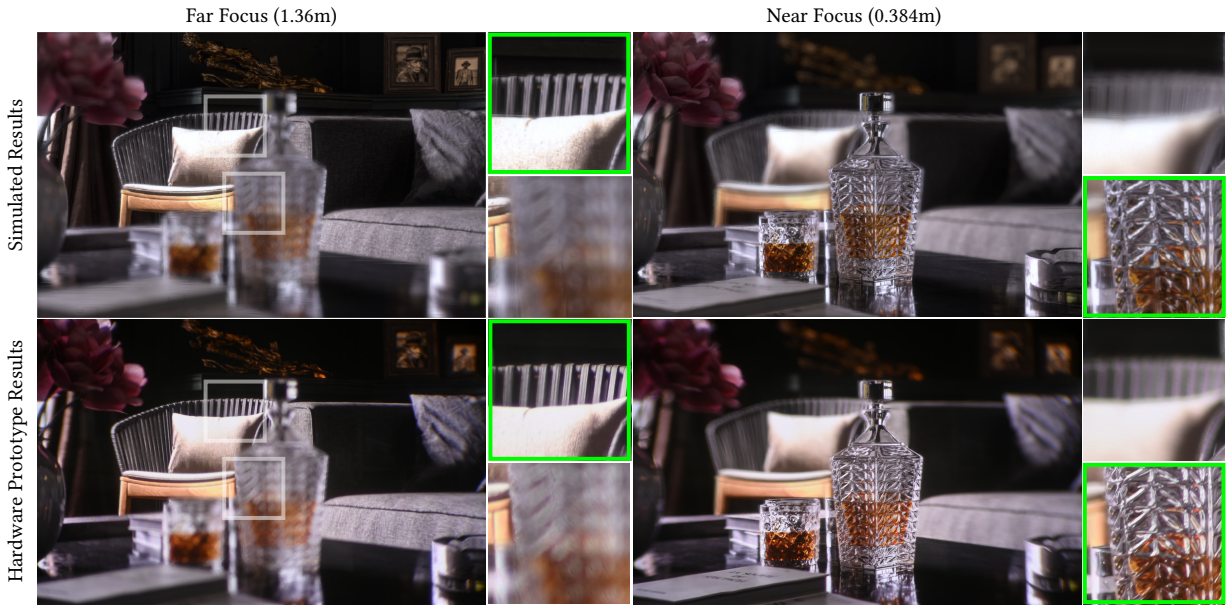

Fig. S6. Simulated vs experimental results on our Split-Lohmann lab prototype. (Credits: 3D scene courtesy of "Entity Designer" at Blender Market)

S2.2 Component Alignment and Calibration

Calibration of the Nominal SLM ramp. The direction of the phase ramp on the SLM has to be aligned with the orientation of the cubic phase plate for it to translate in its diagonal direction, or it will lead to an elliptical defocus blur. To calibrate for the direction of the phase ramp, we display a sparse grid of dots on the OLED and a global phase ramp on the SLM. We then search across varying phase ramp directions and ramp frequencies, and solve for the optimal ramp direction and frequency that would give circularly sharp-focused dots. We repeat this process with the camera focused at different distances. The set of ramp directions that are able to produce these sharp dots would lie on a linear line that tells the rotation of the cubic phase plate and the optimal nominal ramp frequency. We then add this nominal ramp to the phase patterns computed from depth maps to display on the SLM, so that the dots would have circular defocused shape.

Mapping from OLED to SLM. In order to match OLED pixels to SLM pixels, we need to find the homography matrix to perform perspective projection between them. First, we estimated the homography H_1 that maps the OLED display coordinates to camera coordinates. We displayed a binary checkerboard pattern on the OLED with the SLM displaying a constant phase pattern and captured an image with the camera. We solved for H_1 using the input image and the captured image. Second, we estimated the H_2 mapping the SLM coordinates to the camera coordinates. For this, we displayed a binary checkerboard pattern on the SLM, but this time, we had the SLM operating in amplitude mode by rotating the linear polarizer in front of it to 45°. We displayed a constant green image on the OLED to work as a light source and capture an image with the camera. We solved for H_2 using the image on the SLM and the captured image. We obtained the final homography matrix as $H_2H_1^{-1}$ mapping from SLM coordinates to OLED coordinates.

Retardation Calibration of SLM Gamma Curve. As discussed in Section 5.2, we calibrated the SLM gamma curve directly for each color channel on the OLED, without using any additional laser light sources. For each color, we displayed a uniform pattern on OLED and operated the SLM in amplitude mode by placing the polarizer in front of the SLM at 45°. We fit the gamma curve such that, when we displayed 0 to 255 on the SLM, its amplitude response would complete a uniformly mapped $[0, 2\pi]$ period in a cosine curve. Even though the spectrum of each color channel in OLED has a bandwidth as wide as 100 nm, this method can still fit an approximation to the gamma curve.

S2.3 Miscellaneous

To qualitatively better understand how well our prototype in Figure S4 performs, we provide in Figure S6 a comparison of the experimental results to the wave-optics-based simulation results on the same scene. We observe that the experimental results share a high visual quality with the wave-optics based simulation results.

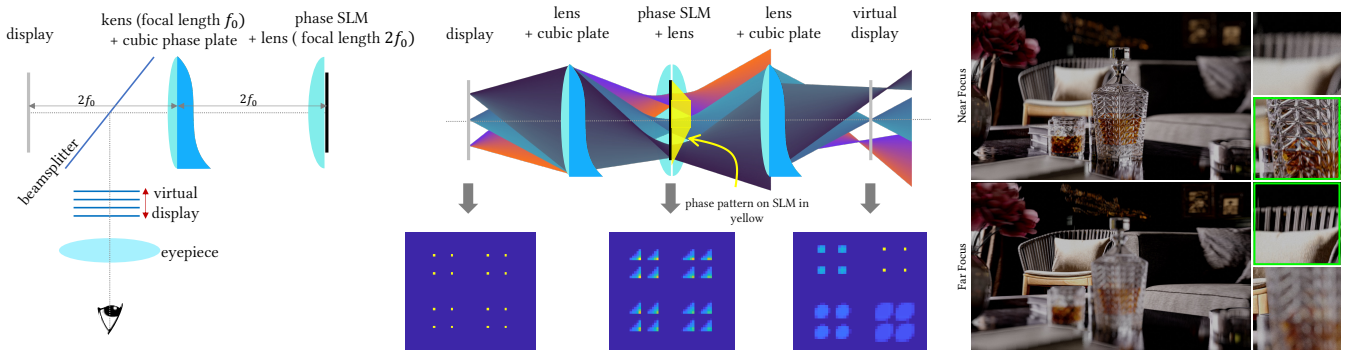

(a) Schematic of compact setup

(b) Ray diagrams and rendered bokeh

(c) Simulated focus stack using Blender

Fig. S7. Proposed design to reducing the overall footprint of the Split-Lohmann display by avoiding 4f systems. (a) Schematic of the system showing how the system avoids the use of a 4f relay; here, to avoid vignetting, we add a field lens on the SLM with precisely calculated focal length so as to avoid field effects. (b) Ray diagrams and rendered bokeh for a sparse scene with points at a different depth. (c) Rendered focus stack for a more complex scene. The renderings were obtained using Blender, with a $f_0 = 100\,\text{mm}$. (Credits: 3D scene courtesy of "Entity Designer" at Blender Market)

S3 COMPACT IMPLEMENTATION DIAGRAMS

We discussed the compact implementation approach in details in Section 6 of our main paper. We further provide in Figure S7 the schematic of the compact setup, the ray diagrams, and the ray-tracing-based simulation results.